Investigating the Thermal Infrared Emission Phase Function of the Lunar Surface Using the the Diviner Lunar Radiometer T. Warren[1], R. Curtis[1], K. Shirley[1], K. Donaldson Hanna[2], E. Sefton-Nash[3], K. Bennett[4], D. Blewett[5], P. O. Hayne[6], B. Greenhagen[5] and N. Bowles[1]. (1) Atmospheric, Oceanic and Planetary Physics, University of Oxford, Dept of Physics, UK, (warren@atm.ox.ac.uk). (2) University of Central Florida, Orlando, FL (3) ESTEC, ESA, Noordwijk, The Netherlands (4) USGS Astrogeology Science Center, Flagstaff, AZ. (5) Johns Hopkins University Applied Physics Lab, Laurel, MD (6). Laboratory for Atmospheric and Space Physics, University of Colorado Boulder.

Introduction: The emission phase function (EPF) – sometimes referred to as the directional emissivity (DE) - describes how thermal infrared (6 – 400 μm) light is scattered or re-emitted from a surface for all possible viewing geometries (Fig. 1). It is similar to the bidirectional reflectance distribution function (BRDF) which describes how a surface reflects visible radiation. The BRDF of different surfaces has been well studied in the past and has been used to constrain the physical nature of planetary surfaces from visible remote sensing missions [1,2]. For flyby missions or missions where observations can only be made of the surface at a few viewing angles, knowledge of the BRDF is particularly important. In this case remote sensing measurements must be normalised through knowledge of the BRDF to a standard viewing angle to allow comparison to standard spectral libraries [2].

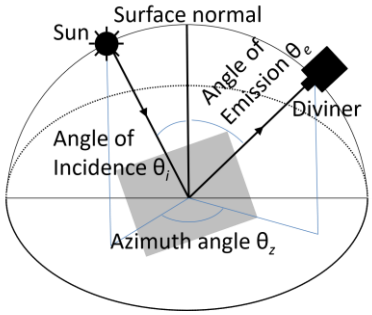

Figure 1: *EPF angle definitions.*

The BRDF is strictly applicable to scattered radiation, e.g. scattered visible solar radiation. This is distinct to the EPF which describes how visible radiation is absorbed by a surface and then re-emitted (typically at TIR wavelengths) [3,4]. It is well known, that the BRDF of a surface is dependent on surface properties such as roughness, porosity, composition and density. Several models, such as Hapke's, attempt to predict the BRDF of a surface based on its physical properties [1]. However, it is often difficult to use a BRDF model to constrain surface properties, since solutions are non-unique [5]. Compared to the BRDF there have been fewer studies of the EPF [1–4]. However, recent laboratory work has shown that the EPF of a surface is dependent on surface roughness and composition [3,4]. Remote sensing measurements of a surface's EPF could therefore be used to constrain its surface roughness or composition. For thermal infrared instruments on flyby missions, knowledge of the EPF is also important for normalising measurements to a standard viewing angle.

As well as providing information on surface properties, the BRDF and the EPF are required inputs for 3D thermal models, which attempt to predict the surface and subsurface temperatures of airless bodies [6–10]. Lunar thermal models constrain where the surface and the subsurface remains cold enough for volatiles, such as water ice, to be trapped. Most thermal models assume the BRDF and EPF of a surface are isotropic, even though laboratory studies have shown the BRDF and EPF are anisotropic [9,10,4]. This invalid assumption could explain a 20-K discrepancy between lunar thermal models and thermal remote sensing measurements in permanently shadowed regions at the lunar poles – where scattered radiation is the dominant input energy. The BRDF of Apollo lunar samples have been measured in the laboratory and remote sensing instruments such as the LROC instrument onboard the Lunar Reconnaissance Orbiter have measured the BRDF of the Moon from orbit [2,10]. However, there have been no published measurements of the lunar EPF.

The Diviner Lunar Radiometer (Diviner) onboard the Lunar Reconnaissance Orbiter [11] has been mapping the Moon's surface temperatures since 2009, primarily with nadir viewing geometry. In 2016, as part of its third extended mission cycle, Diviner began off-nadir observations to measure the EPF of the surface. At a few selected targets, Diviner has now taken enough data at multiple angles to start exploring the lunar EPF.

Diviner Targeted Off-Nadir Dataset: The locations of ten targets for the Diviner off-nadir campaign are given in Table 1. These initial targets were chosen to be typical examples of lunar maria and highland surface roughnesses and composition for investigating the EPF. Diviner is continuing to make off-nadir measurements, measuring the locations given in Table 1 at multiple viewing angles as much as mission planning allows. To give the reader an idea of how complete the EPF measurement is at each location, an angular coverage percentage is provided. This is the percentage of all possible viewing geometries (in 5-degree bins) at that location that have been measured by Diviner.

EPF Measurement Examples: Daytime measurements show that the EPF of the lunar surface is highly anisotropic (Figures 2 and 3), which is significant for

3D thermal models. Initial work including different EPFs using 3D thermal models suggest that the model surface temperature could be changed by up to 50 K [6]. It is easiest to compare EPF of the high-latitude mare and highland region from Table 1, since these regions have the best angular coverage. High-latitude regions have better angular coverage because LRO's polar orbit often passes over these regions. Surprisingly, the Diviner EPF in the highland and mare regions is identical to within 0.05 emissivity units.

Region Description	Lon/Lat	Angular Coverage
Equatorial Highland	141.39 0.36	20% 2,020,458
Equatorial Mare	-0.6 -1.96	15% 2,167,490
Aristarchus Plateau	-51.73 27.36	18% 4,812,426
Kepler Ejecta	-36.53 8.33	12% 2,717,837
Reiner Gamma	-58.98 7.41	1% 10,536
Dufay Albedo Anomaly	170.43 7.65	25% 4,505,391
Cold Spot	151.90 -3.30	22% 2,461,684
High latitude Highland	-109.55 49.55	39% 6,068,198
High latitude Mare	-71.52 52.97	49% 7,746,669
King Crater	119.84 6.60	1% 33549

Table 1: *Initial targets of Diviner's off-nadir campaign. The given coordinate has been viewed at multiple viewing geometries by Diviner. The percentage in the third column is a measure of the completeness of angular coverage available for that target. The number of data points is also provided.*

Conclusions and Future Work.

Daytime off-nadir Diviner measurements show a statistically insignificant difference between the EPF of the lunar highland and the mare regions. Since the EPF is known to be dependent on surface roughness, this could suggest that both regions have equivalent roughness. The scale of roughness to which the EPF is sensitive is debated, but is likely to be the scale at which the lunar surface is thermally insulating ~3 cm. A 3D thermal model of a randomly rough surface has been used to predict the EPF [6], which suggested that the RMS slope of Moon must be ~40° at the 3-cm scale to observe the measured EPF.

Diviner is continuing to make off-nadir measurements at the targets given in table 1. It is also making measurements at 70° emission angle globally across the whole lunar surface. More comparisons between different regions on the lunar surface need to be made to draw any further conclusions. However, the initial measurements show that the EPF is very anisotropic. The next step is to include the Diviner measured anisotropic EPF in 3D thermal models, in order to accurately predict surface and sub-surface temperatures.

L-CIRiS is a thermal infared radiometer payload designed for NASAs LCPS lunar lander program [12]. L-CIRiS will also make thermal EPF measurements on the lunar surface. Comparison between the km scale Diviner measured EPF and the meter scale EPF measured by L-CIRiS will provide further insight into the dominant length scale for the EPF on the lunar surface.

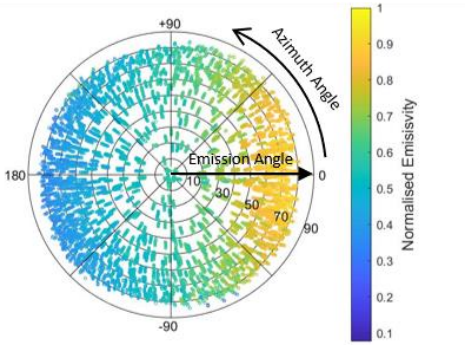

Figure 2: *Diviner-measured EPF at 70° incidence angle for the high-latitude highland target.*

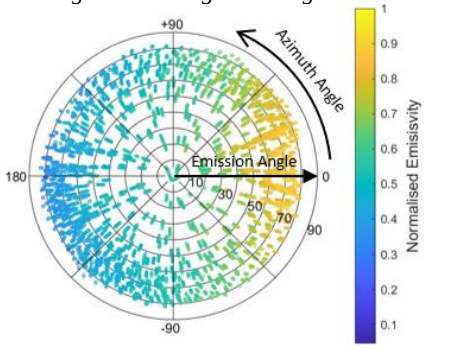

Figure 3*: Diviner-measured EPF at 70° incidence angle for the high-latitude mare target.*

Acknowledgements: Thanks to the UK Science and Technology Facilities Council, UK Space Agency and the Leverhulme Trust for supporting this work.

References: [1] B. Hapke (2012), *Icarus 221*, 1079. [2] H. Sato *et al.* (2014), *JGR 119*. [3] T. Warren *et al.* (2017), *Rev. Sci. Instrum. 88*, 124502. [4] T. Warren *et al.* (2019), *JGR* [5] P. Helfenstein and M. Shepard. (1999), *Icarus 141*, 107. [6] King and Warren et al. (2020), *Planet. Space Sci* 182 104790. [7] A. Vasavada *et al.* (2012), *JGR 117*, E00H18. [8] P. Hayne *et al.* (2015), *Icarus 225*, 58. [9] D. Paige *et al.* (2010) *Science 330*, 479. [10] E. Foote *et al.* (2020), *Icarus 336*, 113456. [11] D. Paige *et al.* (2009), *Space Sci. Rev. 150*, 125. [12] D. Osterman LPSC 2020 #2707